Broadband telecom to mid-infrared supercontinuum generation in a dispersion-engineered Silicon Germanium waveguide

MOHAMED A. ETTABIB[1,*], LIN XU[1], ADONIS BOGRIS[2,3], ALEXANDROS KAPSALIS[2], MOHAMMAD BELAL[1], EMERICK LORENT[4], PIERRE LABEYE[4], SERGIO NICOLETTI[4], KAMAL HAMMANI[5], DIMITRIS SYVRIDIS[2], DAVID P. SHEPHERD[1], JONATHAN H.V. PRICE[1], DAVID J. RICHARDSON[1], AND PERIKLIS PETROPOULOS[1]

[1] *Optoelectronics Research Centre, University of Southampton, Southampton, SO17 1BJ, UK*
[2] *Department of Informatics and Telecommunications, National and Kapodistrian University of Athens, Panepistimiopolis, Ilissia, 15784, Athens, Greece*
[3] *Department of Informatics, Technological Educational institute of Athens, Egaleo, 12210, Athens, Greece*
[4] *CEA-Leti MINATEC Campus, 17 rue des Martyrs 38054 Grenoble Cedex 9, France*
[5] *Laboratoire Interdisciplinaire Carnot de Bourgogne (ICB), UMR 6303 CNRS-Université de Bourgogne, 9 av. A. Savary, BP 47 870, F-21078 Dijon Cedex, France*
[*] *Corresponding author: mae206@orc.soton.ac.uk*

Compiled August 10, 2015

We demonstrate broadband supercontinuum generation (SCG) in a dispersion-engineered silicon-germanium waveguide. The 3-cm long waveguide is pumped by femtosecond pulses at 2.4μm and the generated supercontinuum extends from 1.45μm to 2.79μm (at the -30-dB point). The broadening is mainly driven by the generation of a dispersive wave in the 1.5-1.8μm region and soliton fission. The SCG was modelled numerically and excellent agreement with the experimental results was obtained.

OCIS codes: *(130.3120) Integrated optics devices; (190.4390) Nonlinear optics, integrated optics; (230.7390) Waveguides, planar.*

http://dx.doi.org/10.1364/ao.XX.XXXXXX

Silicon (Si) photonics has witnessed rapid maturity in recent years, mainly due to its potential for high-yield, low-cost CMOS-compatible fabrication of components. At the same time, the high nonlinear refractive index of silicon (n_2 = 4.5x10^{-18} m^2/W), especially when combined with small-dimension, high refractive-index-contrast waveguide geometries that lead to tight mode confinement, makes Si photonic technologies particularly attractive for nonlinear applications. Si-based devices have already been utilized to demonstrate numerous all-optical signal processing applications. Indeed, nonlinear effects such as four-wave mixing (FWM) [1], self-phase modulation (SPM) [2] and Raman amplification [3] have been demonstrated in silicon-on-insulator (SOI) waveguides and nanowires designed for operation in the near-infrared (IR).

Silicon is also an excellent candidate for mid-IR applications, due to its transparency up to 8μm and to the reduced two-photon and free-carrier absorptions at wavelengths beyond 2.2μm. Leveraging on these attributes, moderate to high brightness wide-bandwidth laser sources have been demonstrated based on supercontinuum generation (SCG) in this wavelength region, using waveguides fabricated on either crystalline silicon [4, 5], amorphous silicon [6] or silicon nitride [7]. Furthermore, the development of on-chip sources providing short pulses has driven research towards integrating both the pump source and nonlinear element on the same chip [8].

We have recently reported the first demonstrations of all-optical signal processing using silicon germanium waveguides both in the near- [9] and mid-IR [10]. These demonstrations, along with a detailed study on the optical properties of SiGe waveguides [11], have highlighted that the addition of germanium to silicon can enhance the nonlinear response in comparison to pure silicon, as well as act as an additional valuable design parameter that can impact a host of optical properties (such as linear loss, two-photon absorption (TPA) and dispersion) of the nonlinear waveguide.

In this Letter, we have extended the work presented in [12] where we reported the generation of a broadband supercontinuum (SC) in a dispersion-engineered SiGe waveguide. The waveguide was pumped using femtosecond pump pulses at 2.4μm and the 30-dB bandwidth of the SC extended more than 1330 nm spanning both the mid-IR and the entire telecommunication wavelength window, while maintaining high spectral uniformity. A numerical model was also developed to study the SCG, providing excellent agreement with the experimental data and offering valuable insights into the physical mechanism driving the SC formation.

The SiGe device used was an air-clad waveguide with a 2μm linear taper at each facet to facilitate input coupling. The length of each taper was 0.5 mm and the total device length was 30mm.

The device was grown by reduced-pressure chemical vapor deposition (RPCVD) on a SOI wafer with a 2μm buried oxide layer (BOX). A buffer Si layer was first grown to adjust the SOI layer thickness to the desired value. The waveguide adopted a graded Ge concentration profile which was realized by varying the germanium mass-flow during growth, with the dichlorosilane mass-flow staying constant. The process involved linearly increasing the Ge concentration from 0% to 42% and then reducing it back to pure Si symmetrically (see ref. [10] for further details). The precise concentration and doping profile of Ge are important for achieving the targeted dispersion and modal properties required by the application and were determined taking into account both the design targets and fabrication constraints. The top of the SiGe graded-index layer was lowered by etching while monitoring in situ the Ge content in the etched by-products with mass spectroscopy.

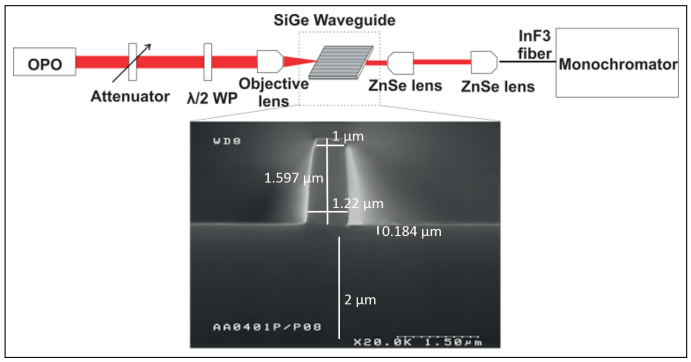

Fig. 1. Experimental setup used for the SC generation experiment. $\lambda/2$ WP: half-wave plate. Inset: Scanning Electron Microscopy (SEM) image of the waveguide.

The waveguide was realized by photolithography and etching. Etching ensured that the thickness of Si on the BOX layer that constituted the slab was 184nm. The control of the Si slab thickness allowed the dispersive and the modal properties of the waveguide to be in line with the design targets. The final fabricated device had an isosceles trapezoidal structure with a vertical height of 1.597μm, a top width of 1μm and a bottom width of about 1.22μm (see inset in Fig. 1). A detailed account of the waveguide design and fabrication process can be found in [10]. Experimental characterization revealed that the waveguide exhibited losses close to 2 dB/cm at 2.4μm, and the simulations predicted a nonlinear coefficient of 24.7/W/m and 23/W/m and a ZDW of 2.1μm and 1.875μm for the TM and TE modes respectively (Fig. 2).

The experimental setup used for the SCG experiment is shown in Fig. 1. An idler-resonant femtosecond optical parametric oscillator (OPO) at 2.4μm was used as the pump source. The OPO was synchronously pumped by a femtosecond Yb-fiber amplifier system providing 130 fs pulses with an average power of 4.5 W at 1050 nm and delivered 90 fs pulses at a repetition rate of 80 MHz with a maximum average power of 300 mW for the idler at 2.4μm and a near diffraction-limited ($M_2 \sim 1.05$) beam quality [13]. The OPO pulses were coupled into the SiGe waveguide using a free-space objective lens resulting in approximately 25 dB coupling loss. The low coupling efficiency can be attributed to both poor facet cleaving and non-optimized optics used for coupling light into the waveguide. By optimizing these two parameters, a coupling loss figure of 9-10 dB is expected to be achieved as reported in [10]. A half-wave plate was used to

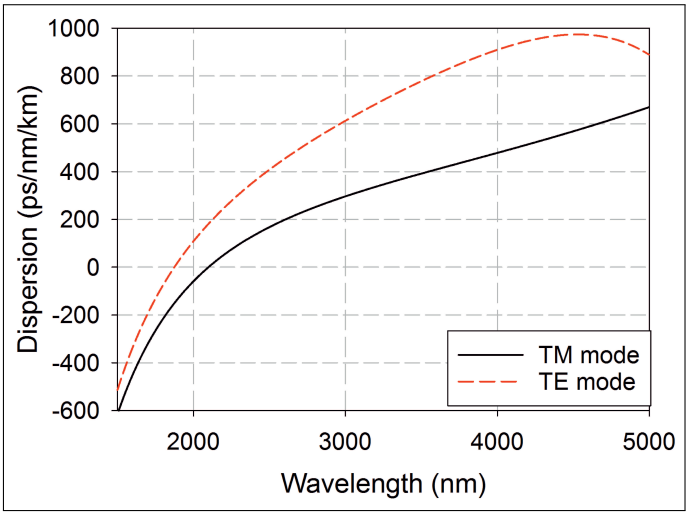

Fig. 2. The simulated chromatic dispersion profile of the TE (red) and TM (black) modes of the SiGe waveguide.

vary the polarization alignment of the pump such that the TM mode of the waveguide was efficiently excited. The maximum coupled peak pump power into the waveguide was estimated to be 120 W, corresponding to a pulse energy of 9.5 pJ. The average supercontinuum power generated at the output of the waveguide was 0.15mW giving rise to a conversion efficiency of approximately 16% compared to launched power from the OPO. At the output of the waveguide, the light was collected, collimated and re-focused into a commercial mid-IR fluoride fiber using a pair of ZnSe lenses. The optical spectrum was measured with a monochromator (TMc300, Bentham Ltd.) and a liquid-nitrogen-cooled InSb detector.

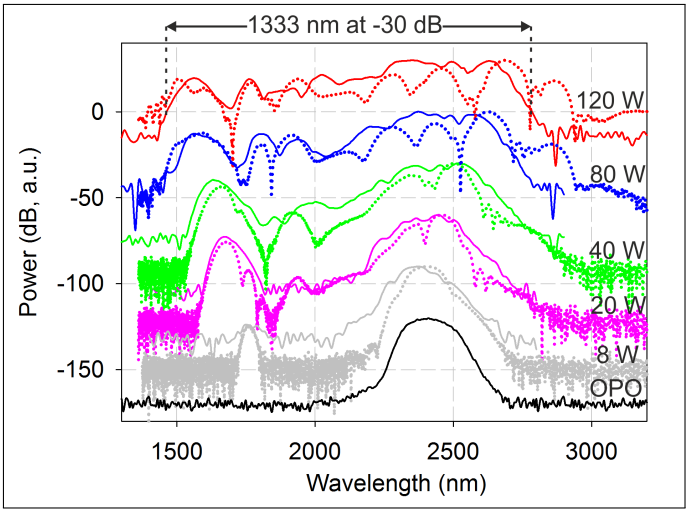

Fig. 3. The evolution of the spectrum as a function of the coupled peak power into the waveguide as obtained experimentally (lines) and from numerical modelling (dotted lines). Successive spectral traces are shifted by 30dB for clarity.

Figure 3 shows the output spectra recorded on the monochromator for various amounts of coupled peak power. At the maximum coupled peak power of 120 W, a broadband SC was observed at the output of the waveguide with a 30-dB bandwidth extending from 1.45μm to 2.79μm, and a 10-dB bandwidth of

520 nm, which is one of the broadest 10-dB bandwidths demonstrated with silicon-based devices. This was achieved by pumping the SiGe waveguide in the anomalous dispersion regime, therefore favoring the formation of a wider spectrum, as well as operating beyond the TPA cut-off wavelength, thus reducing the detrimental effects of nonlinear losses.

A numerical model simulating the SC broadening in the SiGe waveguide was developed in order to verify the experimental results and to gain an understating of the dominant physical mechanisms that drive the spectral broadening. The model used values of the linear and nonlinear refractive index of the SiGe alloy that had been verified experimentally in refs. [10] and [11]. Furthermore, the femtosecond OPO pulses necessitated the inclusion of both three photon absorption (3PA) and free carrier effects, which have been shown to be the dominant nonlinear loss mechanisms at wavelengths beyond 2.2μm. The Raman effect was neglected, since it plays a minor role in silicon-based waveguides due to its relatively narrow gain spectrum [14].

The propagation of the ultra-short pulses along the SiGe waveguide can be satisfactorily described by the nonlinear Schrödinger equation as follows:

$$\frac{\partial A}{\partial z} = -\frac{\alpha}{2}A + \sum_{k=2}^{\infty} i^{k+1}\frac{\beta_k}{k!}\frac{\partial^k A}{\partial t^k} + \left(1+\frac{i}{\omega_0}\frac{\partial}{\partial t}\right)\left(i\gamma|A|^2A - \frac{\gamma_{3PA}}{3A_{eff}^2}|A|^4A\right) - \frac{\sigma}{2}(1+i\mu)N_cA \quad (1)$$

In Eq. 1, $A(z,t)$ is the envelope of the electric field, α is the attenuation coefficient of the waveguide, β_k are the dispersion coefficients at the central frequency ω_0 of the pulse, γ_{3PA} is the 3PA coefficient, σ and μ are the free-carrier absorption (FCA) cross section and free-carrier dispersion (FCD) parameters respectively, and $\gamma = \omega_0 n_2/cA_{eff}$ is the effective nonlinearity coefficient of the waveguide, where n_2 is the nonlinear index coefficient, and A_{eff} is the effective area of the waveguide mode. The modeling of the free carrier density evolution and the values of μ, σ and γ_{3PA} parameters are identical to that of ref. [5]. The dispersion coefficients were extracted by the effective refractive index calculated from 1.3μm to 7μm with the use of a mode solver in COMSOL. Instead of numerically approximating the higher orders of dispersion, the infinite series of dispersion terms in Eq. 1 was calculated with a higher accuracy following the equation:

$$F\left(\sum_{k=2}^{\infty} i^{k+1}\frac{\beta_k}{k!}\frac{\partial^k A}{\partial t^k}\right) = \Big[\beta(\omega) - \beta(\omega_0) - \beta_1(\omega_0)(\omega-\omega_0)\Big]F\Big(A(t)\Big) \quad (2)$$

where $\beta(\omega) = n_{eff}(\omega)\omega/c$, $\beta_1(\omega) = d\beta/d\omega$ and F is the Fourier transform operator.

Using the same mode solver, A_{eff} was found to be 1.19μm^2. The real part of the nonlinear index coefficient n_2 was estimated to be 11x10^{-14} cm^2/W, following ref. [15] and taking into account the gradient concentration profile of germanium in the waveguide. The model ignored the two-photon-absorption effect in the near-IR and the dispersion of nonlinearity (i.e. the dependence of the n_2 parameter on wavelength [16]) along the entire wavelength span as their inclusion in Eq. 1 is not a straightforward task and because the seed wavelength where the pulse has highest intensity was above the TPA cut-off.

The free-carrier density N_c is modeled by the following rate equation:

$$\frac{dN_c}{dt} = \frac{\gamma_{3PA}}{3hf_0}\frac{|A|^6}{A_{eff}^3} - \frac{N_c}{t_{eff}} \quad (3)$$

where t_{eff} is the effective carrier lifetime considering a characteristic value of 10 ns, based on ref. [5].

Figure 3 (dotted lines) shows the simulated SC spectra at various peak-power levels. The simulated spectra reveal that the initial spectral broadening taking place at low pump powers, is driven by SPM. As the power increases, dispersive-wave generation is observed in the near-IR (1.5-1.8μm region) and soliton fission starts to dominate, causing all those spectral features to merge and explaining the broadband nature of the generated SC radiation. A very good agreement between experimental and numerically simulated values is obtained. The main deviation between simulations and experiments in Fig. 3 is observed at high peak powers and could be attributed to nonlinearity dispersion which is not considered in the model. As such, the model does not account for the reduced nonlinearity of the waveguide at longer wavelengths and thus slightly over-estimates the extent of the broadening. Neglecting the emergence of TPA effects at the telecommunication wavelengths does not seem to impact the agreement between the experimental data and the simulations.

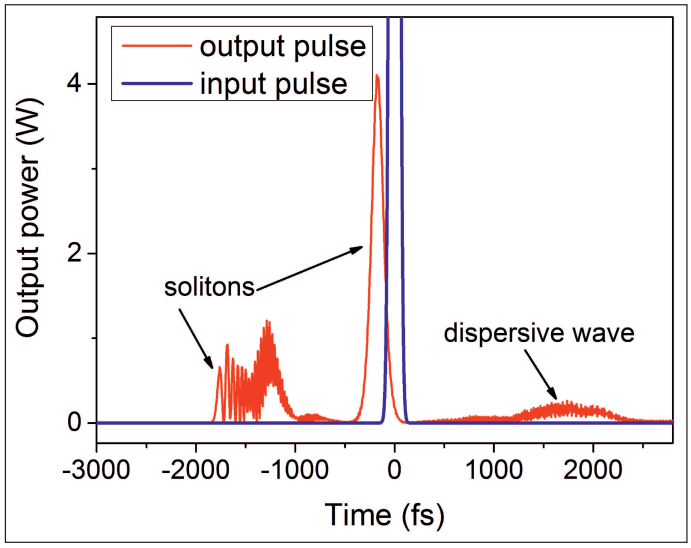

Fig. 4. The simulated temporal profile for 80 W of peak power, at the input and after propagation in 3 cm of the waveguide.

The SC was also studied in the time domain. Figure 4 shows the simulated temporal profile in the case of 80 W of peak power, while Fig. 5 depicts the longitudinal evolution of the optical power as a function of time at the same peak power level. In both figures, the findings above are confirmed, where the dispersive and soliton components can again be clearly observed. The main pulse is seen to break off into three lower order soliton pulses and a dispersive pulse as it propagates further into the waveguide, with the dispersive pulse broadening steadily as it propagates longitudinally (Fig. 5). This is in accordance with the theoretically analyzed soliton order following the condition $N^2 = Re(\gamma)P_0T_0^2/|\beta_2|$ [14]. For a peak power 80 W, the order of soliton of $N \sim 3$ is consistent with both Fig. 5 and Fig. 6, as three solitons can be identified within the first 7 mm of the waveguide.

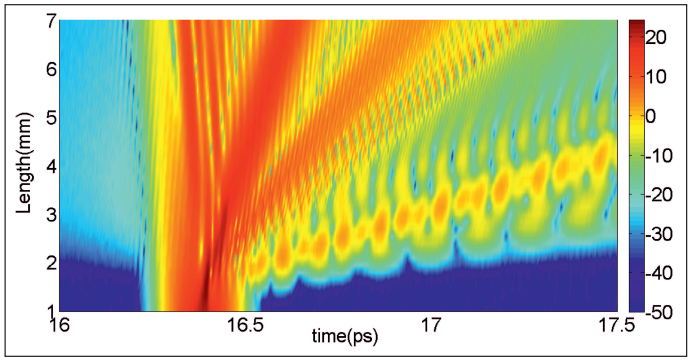

Fig. 5. Longitudinal evolution of the optical power as a function of time at a peak power of 80 W. The color-bar shows the power density using a dBm scale.

The evolution of the SCG as a function of the waveguide length calculated for the case of 80-W peak power is shown in Fig. 6. The figure shows that the SC forms fully within the first 2.5 mm of the waveguide, highlighting the prospect of the technology for providing even more miniaturized broadband sources. Furthermore, the use of a more compact chip would increase significantly the supercontinuum power at the output and thus improve the efficiency of the SCG system accordingly.

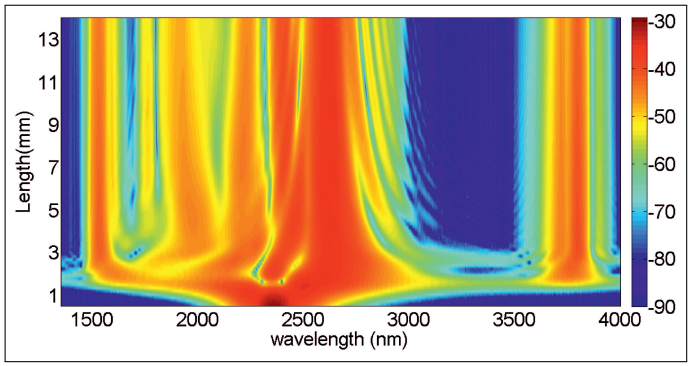

Fig. 6. The evolution of the SCG power density along the waveguide as a function of wavelength at a peak power of 80 W. The color-bar shows the power density using a dBm scale.

In conclusion, this Letter has demonstrated the generation of a continuous and highly uniform SC extending from telecommunications to mid-IR wavelengths. A numerical study modelling the experimental conditions was conducted, revealing a close agreement between the experimental and numerical findings. The study revealed that the origin of the SC broadening mainly stems from the generation of dispersive wave and soliton fission. The results reported here emphasize the versatility of SiGe devices for nonlinear applications over a wide range of wavelengths. The inclusion of Ge in the waveguides facilitates flexible dispersion engineering and enhances the effective nonlinear coefficient.

FUNDING INFORMATION

Funding. The European Communities Seventh Frame-work Programme FP7/2007-2013 under Grant 288304 (STREP CLARITY); The Photonics Hyperhighway Programme Grant (EPSRC grant EP/I01196X). The data for this paper can be found at DOI:10.5258/SOTON/377002.

REFERENCES

1. B. Lee, A. Biberman, A. Turner-Foster, M. Foster, M. Lipson, A. Gaeta, and K. Bergman, IEEE Photon. Technol. Lett. **21**, 182–184 (2009).
2. E. Dulkeith, Y. A. Vlasov, X. Chen, N. C. Panoiu, and J. Richard M. Osgood, Opt. Express **14**, 5524–5534 (2006).
3. H. Rong, A. Liu, R. Jones, O. Cohen, D. Hak, R. Nicolaescu, A. Fang, and M. Paniccia, Nature **433**, 292–294 (2005).
4. B. Kuyken, T. Ideguchi, S. Holzner, M. Yan, T. W. Haensch, J. V. Campenhout, P. Verheyen, R. G. F. Baets, G. Roelkens, and N. Picqué, in "Conference on Lasers and Electro-Optics (CLEO), San Jose, CA," (2014), p. ATh4P.2.
5. R. K. W. Lau, M. R. E. Lamont, A. G. Griffith, Y. Okawachi, M. Lipson, and A. L. Gaeta, Opt. Lett. **39**, 4518–4521 (2014).
6. U. D. Dave, S. Uvin, B. Kuyken, S. Selvaraja, F. Leo, and G. Roelkens, Opt. Express **21**, 32032–32039 (2013).
7. R. Halir, Y. Okawachi, J. S. Levy, M. A. Foster, M. Lipson, and A. L. Gaeta, Opt. Lett. **37**, 1685–1687 (2012).
8. K. Saha, Y. Okawachi, B. Shim, J. S. Levy, R. Salem, A. R. Johnson, M. A. Foster, M. R. E. Lamont, M. Lipson, and A. L. Gaeta, Opt. Express **21**, 1335–1343 (2013).
9. M. A. Ettabib, K. Hammani, F. Parmigiani, L. Jones, A. Kapsalis, A. Bogris, D. Syvridis, M. Brun, P. Labeye, S. Nicoletti, and P. Petropoulos, Opt. Express **21**, 16683–16689 (2013).
10. K. Hammani, M. A. Ettabib, A. Bogris, A. Kapsalis, D. Syvridis, M. Brun, P. Labeye, S. Nicoletti, and P. Petropoulos, Opt. Express **22**, 9667–9674 (2014).
11. K. Hammani, M. A. Ettabib, A. Bogris, A. Kapsalis, D. Syvridis, M. Brun, P. Labeye, S. Nicoletti, D. J. Richardson, and P. Petropoulos, Opt. Express **21**, 16690–16701 (2013).
12. M. A. Ettabib, L. Xu, A. Bogris, A. Kapsalis, M. Belal, E. Lorent, P. Labeye, S. Nicoletti, K. Hammani, D. Syvridis, J. Price, D. J. Richardson, and P. Petropoulos, in "Optical Fiber Communication (OFC) Conference, Los Angeles," (2015), p. Tu2C.5.
13. L. Xu, J. S. Feehan, L. Shen, A. C. Peacock, D. P. Shepherd, D. J. Richardson, and J. H. Price, Appl. Phys. B (2014).
14. L. Yin, Q. Lin, and G. P. Agrawal, Opt. Lett. **32**, 391–393 (2007).
15. N. K. Hon, R. Soref, and B. Jalali, J. Appl. Phys. **110**, 011301 (2011).
16. B. Adonis, A. Kapsalis, K. Hammani, M. Ettabib, M. Brun, P. Labeye, S. Nicoletti, P. Petropoulos, and D. Syvridis, in "European Conference on Optical Communication (ECOC), Cannes," (2014), p. Mo.3.7.5.